Nonlinear Spectral Mixing Models for Vegetative and Soil Surfaces

Christoph C. Borel and Siegfried A. W. Gerstl**

In this article we apply an analytical solution of the radiosity equation to compute vegetation indices, reflectance spectra, and the spectral bidirectional reflectance distribution function for simple canopy geometries. We show that nonlinear spectral mixing occurs due to multiple reflection and transmission from surfaces. We compare radiosity-derived spectra with single scattering or linear mixing models. We also develop a simple model to predict the reflectance spectrum of binary and ternary mineral mixtures of faceted surfaces. The two-facet model is validated by measurements of the reflectance.

INTRODUCTION

Vegetation indices have been widely used and related to biophysical canopy parameters such as leaf area index (e.g., Goel, 1988; Asrar, 1989; Baret and Guyot, 1991). They are usually based on ratios of two measured radiances that relate to spectral reflectances from two spectral bands as shown by Tucker (1979) or a combination of multiple bands (see Kauth and Thomas, 1976; Jackson, 1983). Operational satellite sensors such as Landsat TM, SPOT, and AVHRR have multiple spectral bands which are used not only to classify pixels into distinct surface classes, e.g., vegetation, bare soil, water etc., but also to estimate fractions of basic classes within each pixel (e.g., Huete, 1986; Satterwhite and Henley, 1987; Smith et al., 1990a,b; Roberts, 1991). With the deployment of airborne hyper-spectral sensors such as the Airborne Imaging Spectrometer (AIS) (Vane and Goetz, 1988) and the Airborne Visible / Infrared Imaging Spectrometer (AVIRIS) (Green, 1991) and projected sensors such as the High-Resolution Imaging Spectrometer (HIRIS) (Goetz, 1987; Dozier and Goetz, 1989) and the Moderate Resolution Imaging Spectrometer (MODIS) (Salomonson et al., 1989) in the EOS program, we must develop new and physically based scattering models to take advantage of the hyper-spectral information.

Linear spectral factor analysis or un-mixing theory has been widely used to compute the abundance or percentage of soil or mineral components in a surface cover (e.g., Huete et al., 1985; Huete, 1986; Smith et al., 1990a, b; Roberts, 1991). With the Airborne Visible / Infrared Imaging Spectrometer (AVIRIS) (Green, 1991) it is now possible to test various spectral models.

Others observed that no linear combination of spectra can fully represent the measured composite scene spectra and that residuals can be quite large (see Roberts et al., 1990; 1991). The residual or remaining part has been attributed to the "shade" in the scene (Roberts, 1991) and is assumed to be a constant. Measured reflectances for broad leaf trees like sugar maple show that the NIR reflectance at the branch level is higher than at the leaf level (Williams, 1991). We will show that this effect is due to multiple reflections between leaves.

In this article, we will present a novel method to compute the reflectance spectrum and the spectral bidirectional reflectance distribution function for two simple canopy geometries. The method used is based on the radiosity method (see Hottel and Sarofim, 1967; Gerstl and Borel, 1990; Borel et al., 1991), and is in principle applicable to many complex surface types and also volumetric scattering (see Rushmeier and Torrance, 1987; Borel and Gerstl, 1991).

To illustrate the nonlinear spectral mixing effect, we start with a simple model, a single-layer of vegetation above soil. The model used in this article has already been described in detail in Borel et al. (1991) but will be briefly summarized. We demonstrate that the nonlinear spectral mixing is due to multiple reflections and transmissions between the leaf layer and soil.

*Non-Proliferation and International Security Division, Los Alamos National Laboratory

Address correspondence to Christoph C. Borel, Non-Proliferation and International Security Division, Los Alamos National Lab., MS D436, Los Alamos, NM 87545.

Received 29 December 1992; revised 5 June 1993.

0034-4257 / 94 / $7.00

655 Avenue of the Americas, New York, NY 10010

Next, a layered canopy model is described and used to compute vegetation indices and the spectral BRDF using analytical solutions derived in Borel et al. (1991). The method presented can also be applied to rough surfaces, and in the final section a simple model for rough soil is developed and validated. Other researchers have noted that nonlinear spectral mixing occurs when two or more substances are mixed and the reflectance spectrum is measured (see Nash and Conel, 1974; Hapke, 1981; Johnson et al., 1983). We compute the reflectance of binary and ternary mineral mixtures using the radiosity method.

NONLINEAR MIXING IN A SINGLE LAYER CANOPY USING RADIOSITY

In this section we repeat some of the derivations from Borel et al. (1991) because there was a typographical error in one of the radiosity equations, which caused the analytical solution to be wrong as well. Analytic expressions for the BRDF in the hot spot direction and away from it are also derived. A simple linear reflectance model for soil is used to compute the reflectance. Vegetation indices are computed using two wavelengths in the red and near-infrared part of the spectrum.

Review of the Single Layer Radiosity Model

For a single-layer canopy of horizontal and nonoverlapping Lambertian disks above a Lambertian surface (see Fig. 1), the three radiosity equations can be written down by heuristic arguments. From Borel et al. (1991) we obtain equations for the layer-averaged radiosity of the top surface of the leaf layer (B_1), the underside (B_2), and the ground surface (B_3):

$$B_1 = \rho\ \text{lai}\ E_0 + \tau\ \text{lai}\ B_3,$$
$$B_2 = \tau\ \text{lai}\ E_0 + \rho\ \text{lai}\ B_3,$$
$$B_3 = \rho_s(1 - \text{lai})E_0 + \rho_s B_2, \qquad (1)$$

where E_0 is the total incident solar power per unit area in (W m^{-2}), lai is the leaf area index of a leaf layer without overlapping leaves in (m^2 m^{-2}), ρ and τ are the hemispherical reflectance and transmittance of the leaves, and ρ_s is the soil reflectance. Note that in this case the lai is also equal to the fractional leaf cover.

The analytical solution of the set of linear equations (1) is

$$B_1 = E_0\ \text{lai}\ \rho + E_0\ \text{lai}\ \tau\rho_s\left[\frac{1 + \text{lai}(\tau - 1)}{1 - \rho\rho_s\ \text{lai}}\right],$$
$$B_2 = E_0\ \text{lai}\left[\frac{\tau + \rho\rho_s(1 - \text{lai})}{1 - \rho\rho_s\ \text{lai}}\right],$$
$$B_3 = E_0\rho_s\left[\frac{1 + \text{lai}(\tau - 1)}{1 - \rho\rho_s\ \text{lai}}\right]. \qquad (2)$$

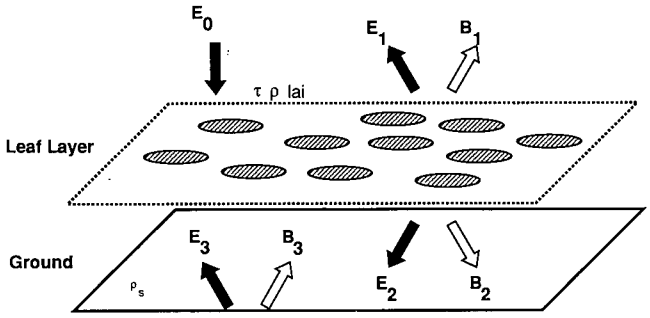

Figure 1. Geometry for a single-layer of horizontal nonoverlapping Lambertian disks above a Lambertian reflecting surface. The black arrows indicate the single scattering components E and the white arrows indicate the radiosities B.

Computing the Spectral Bidirectional Reflectance Distribution Function (BRDF) for a Single Layer Canopy

The BRDF of a single-layer canopy is given by adding all visible surface radiosities for a given sun angle (θ_i, φ_i) and view direction (θ_r,φ_r) or

$$f(\theta_i, \varphi_i; \theta_r, \varphi_r) = \frac{1}{E_0}\frac{1}{\pi}[P_{\text{leaf}}^{\text{sunlit}}(\theta_r, \varphi_r)B_{\text{leaf}}^{\text{sunlit}} + P_{\text{soil}}^{\text{sunlit}}(\theta_r, \varphi_r) \times B_{\text{soil}}^{\text{sunlit}} + P_{\text{soil}}^{\text{shade}}(\theta_r, \varphi_r)B_{\text{soil}}^{\text{shade}}], \qquad (3)$$

where the radiosity on a sunlit leaf is given by

$$B_{\text{leaf}}^{\text{sunlit}} = B_1 / \text{lai} \qquad (4)$$

and the radiosities on the sunlit and shaded soil areas are given by

$$B_{\text{soil}}^{\text{sunlit}} = \rho_s E_0 + \rho_s B_2 \qquad (5)$$

and

$$B_{\text{soil}}^{\text{shade}} = \rho_s B_2. \qquad (6)$$

By definition of the leaf area index, the probability of seeing a sunlit leaf is

$$P_{\text{leaf}}^{\text{sunlit}} = \text{lai}. \qquad (7)$$

One can show that the BRDF of a single layer of horizontal leaves asymptotically reaches a constant value away from the hot spot ($\theta_r \neq \theta_i, \varphi_r \neq \varphi_i$) and peaks in the hot spot direction ($\theta_r = \theta_i, \varphi_r = \varphi_i$) (see Borel et al., 1991). For the hot spot direction no shaded ground is visible; therefore,

$$P_{\text{soil}}^{\text{shade/hot spot}} = 0, \qquad (8)$$

and

$$P_{\text{soil}}^{\text{sunlit/hot spot}} = 1 - \text{lai}. \qquad (9)$$

Away from the hot spot direction, the probability of seeing sunlit ground is given by the product of the probability of sunlit ground and the probability of seeing through the leaf layer or

$$P_{\text{soil}}^{\text{sunlit}} = (1 - \text{lai})^2, \qquad (10)$$

and the probability of seeing shaded soil is given by the product of shaded ground area density and the probability of seeing through the leaf layer or

$$P_{\text{soil}}^{\text{shade}} = \text{lai}(1 - \text{lai}). \tag{11}$$

Using Eqs. (4)–(11) in Eq. (3), we get for the hot spot direction

$$f(\theta_r = \theta_i, \varphi_r = \varphi_i) = \frac{1}{E_0}\frac{1}{\pi}[B_1 + \rho_s(1 - \text{lai})(E_0 + B_2)], \tag{12}$$

and for the directions away from the hot spot

$$\begin{aligned} f(\theta_r \neq \theta_i, \varphi_r \neq \varphi_i) &= \frac{1}{E_0}\frac{1}{\pi}[B_1 + (1 - \text{lai})B_3] \\ &= \frac{1}{E_0}\frac{1}{\pi}[B_1 + \rho_s(1 - \text{lai})^2 E_0 \\ &\quad + \rho_s(1 - \text{lai})B_2]. \end{aligned} \tag{13}$$

In the solution of the radiosity equations (2) we find terms of the form

$$\frac{1}{1 - \rho\rho_s\,\text{lai}}, \tag{14}$$

which represent multiple reflections between the leaf layer and soil. Expression (14) is a quadratic summation:

$$\frac{1}{1 - \rho\rho_s\,\text{lai}} = 1 + \rho\rho_s\,\text{lai} + (\rho\rho_s\,\text{lai})^2 + (\rho\rho_s\,\text{lai})^3 + \cdots \tag{15}$$

and thus the BRDFs in Eqs. (12) and (13) are a nonlinear function of the reflectances of the vegetation and the soil. Thus we define a nonlinear spectral mixing model as a model which contains products of reflectances. It should be noted that Eqs. (12) and (13) can be solved analytically for lai, ρ and ρ_s.

Numerical Results for the Single-Layer Canopy

In this subsection we will compare the classic linear mixture model and the radiosity mixture model with some measured leaf spectra (Staenz, 1991) of cotton plants. The conical/bihemispherical spectral reflectance and transmittance of a cotton leaf was measured shortly after removing the leaf from a mature cotton plant. The instrument, a spectro-radiometer (LICOR-1800), measured the reflectance and transmittance from 300 nm to 1100 nm with a useful range from 400 nm to 1100 nm. The measured spectra are shown in Figure 2. Notice that we use the left vertical axis for the reflectance curve and the right vertical axis for transmittance. The vertical distance between the curves indicates the amount of absorption in a leaf which is small for wavelengths greater than 730 nm. To make the nonlinear effects on the canopy BRDF more easily understood, we approximate the soil reflectance by a linear function:

$$\rho_s(\lambda) = a + b(\lambda - 400)/700, \tag{16}$$

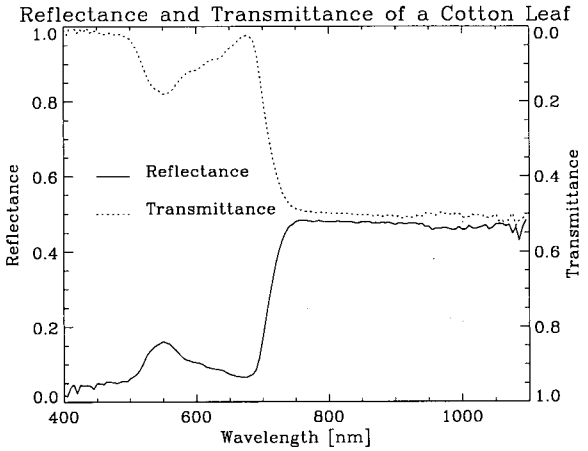

Figure 2. Reflectance and transmittance of a mature cotton leaf (note the different axes for ρ and τ).

where λ is the wavelength in nm. The coefficients a and b were chosen to approximate a background of brown leaf litter or soil. The coefficients for the ground reflectance were $a = 0.2$ and $b = 0.6$. We also varied the leaf area index lai from 0.0625 to 0.9375 in steps of 0.125, and the results are shown in Figure 3.

The linear mixing model assumes that the fraction of visible leaves is given by the lai and that the fraction of visible sunlit ground is given by $(1 - \text{lai})^2$ for a viewing direction far away from the hot spot direction. Thus the linear mixing BRDF is given by

$$f(\theta_r \neq \theta_i, \varphi_r \neq \varphi_i) = \frac{1}{\pi}[\text{lai}\,\rho + (1 - \text{lai})^2\rho_s]. \tag{17}$$

Note that this linear (no products of reflectances) mixing model takes shading of the ground into account. Usually the shadow fraction is not taken into account and only recently Roberts et al. (1990) and Roberts (1991) have used the shadow fraction in spectral mixture analysis as an additional endmember. In the hot spot direction, the BRDF dominates all displayed curves because no shadows are visible. For low reflectances (e.g., in the visible) the higher order terms in Eq. (15) are negligible. In the region of the green reflectance peak near 550 nm, there is a small difference between the linear mixing model and the radiosity mixing model. For high reflectances (e.g., in the near infrared, $\lambda > 700$ nm, for $\rho > 0.3$ and $\rho_s > 0.3$) the higher-order terms contribute more to the calculated radiosity and therefore increase the BRDF significantly. The difference between the two models is a function of the leaf area index and reaches a maximum for an lai of about 0.5. The hot spot BRDF is always higher than the off hot spot BRDF and the difference increases with increasing leaf and/or soil reflectance. In the near infrared the radiosity method yields BRDFs almost twice as high as with the linear mixing model. This fact was confirmed experimentally by Roberts (1992).

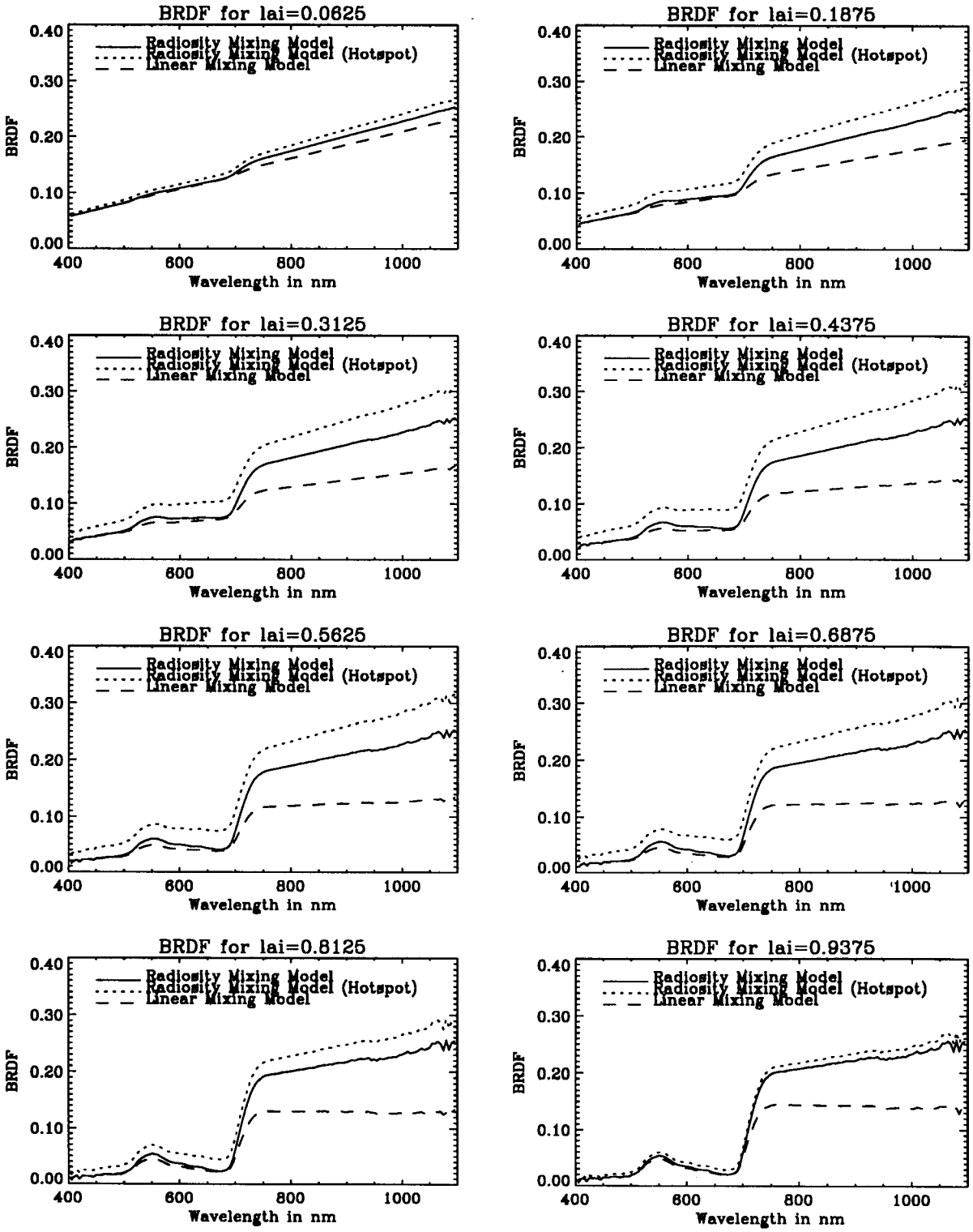

Figure 3. Spectral BRDF for a single-layer canopy above ground as a function of leaf area index.

Vegetation Indices and Nonlinear Mixing

Vegetation indices have been widely used and related to bio-physical parameters such as the total leaf area index (LAI) (see, e.g., Huete et al. 1985; Goel, 1988; Asrar, 1989; Smith et al. 1990a,b; Cihlar et al. 1991; Baret and Guyot, 1991; and many others). The vegetation index has been shown by Jasinski (1990) to depend also on canopy cover, soil albedo, solar and view angle, and pixel scale. From our model it is clear that the relationship between a vegetation index, LAI, and the

Table 1. Some Commonly Used Vegetation Indices

Vegetation Index	*Formula*
Normalized difference vegetation index (NDVI)	(NIR – RED) / (NIR + RED)
Vegetation index (VI)	NIR / RED
Soil-adjusted vegetation index (SAVI)	$\frac{3}{2}$[(NIR – RED) / (NIR + RED + 0.5)]

vegetation and soil reflectances is nonlinear [see eq. (15)]. We have computed various vegetation indices (e.g., Baret and Guyot, 1991), as shown in Table 1.

For the RED reflectance we chose $\lambda = 650$ nm and for the near infrared (NIR), we selected $\lambda = 900$ nm and the parameters listed in Table 2 to match experiments performed by Huete et al. (1985). In Figure 4 we show a scatter plot for the RED and NIR channel. Notice that in this representation the linear mixing model [Eq. (17)] shows a nonlinear curvature because of the quadratic term of lai in Eq. (17). Experimental results by Huete et al. (1985) do not follow the curve of the linear mixing model and rather show a curve as predicted by the single-layer radiosity method. Note that Huete et al.'s data is expressed as fractional leaf cover in percent. In order to compare a one-layer model to the measured data, we use the lai for one layer to represent the green fraction. In reality Huete et al.'s data was measured for canopies with a total lai from 0 to 4. In the hot spot direction the points between the 100% soil and 100% vegetation point (a layer of vegetation material without holes) describe an arc which is very similar to experiments performed by Roberts (1991). It is very interesting to note that RED / NIR scatter point for the radiosity model for a full leaf layer lies separated from the simple linear mixing model. The radiosity derived reflectances lie close to a line connecting the 100% leaf cover and 100% soil points. The symbols denote measurements and computed RED / NIR reflectance for a fractional green cover or in our model for lai = 0., .2, .4, .6, .75, .9, 1.. The spacing between the points increases from a full vegetative cover to a bare soil and is very similar to reported experimental results by Huete et al. (1985) and Satterwhite and Henley (1987). The former are drawn in Figure 4.

In Figure 5 we plot three vegetation indices: NDVI, VI, and SAVI for the above case. Note that the SAVI index is very similar for the radiosity derived indices for the hot spot and off hot spot direction. All used vegetation indices show quite large differences between the radiosity based nonlinear mixing model and the linear mixing model. Also, the NDVI-derived leaf area index from the simple mixture model is always about 0.1 to 0.2 larger than the radiosity based NDVI.

Table 2. Parameters Used in Radiosity Calculation

Parameter	*RED (650 nm)*	*NIR (900 nm)*
ρ	0.0731	0.4661
τ	0.0583	0.5000
ρ_s	0.33	0.3700

RADIOSITY MIXING MODEL FOR A LAYERED CANOPY

In this section we use the previously derived analytical solution in Borel et al. (1991) for the N-layer model to derive BRDF values. Each layer is characterized by its leaf area index lai, the leaf reflectance ρ and the leaf transmittance τ. The ground has a reflection coefficient ρ_s. The upward radiance I_1^+ above the top layer can then be used to compute the BRDF in the following way:

$$f(\theta_r \neq \theta_i, \varphi_r \neq \varphi_i) = I_1^+ / E_0. \qquad (18)$$

We have also shown that an analytical solution for the radiances I_n^+ and I_n^-, $n = 1, 2, 3, \ldots, N$ exists and has the form

Figure 4. Scatter plot for red and near infrared channel as a function of the green cover fraction of (in the case of the single layer model) the leaf area index in steps 0%, 20%, 40%, 60%, 75%, 90%, 95%, and 100% and compared to measured data from Huete et al., (1985).

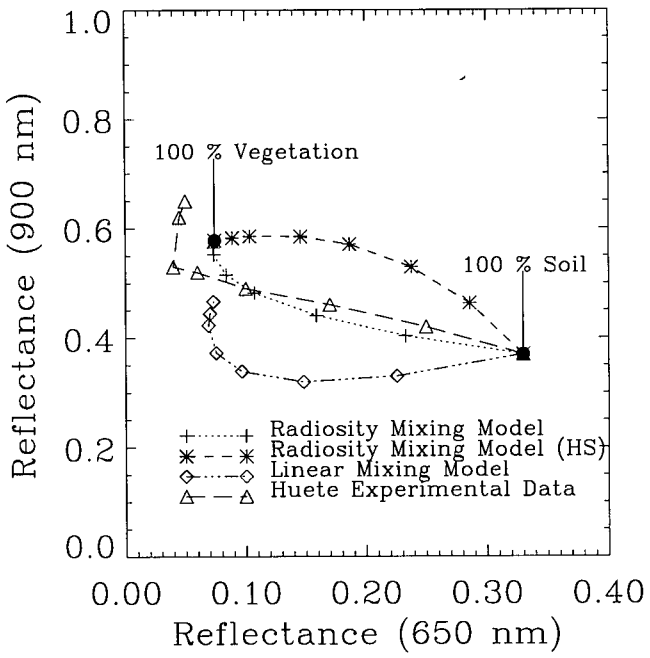

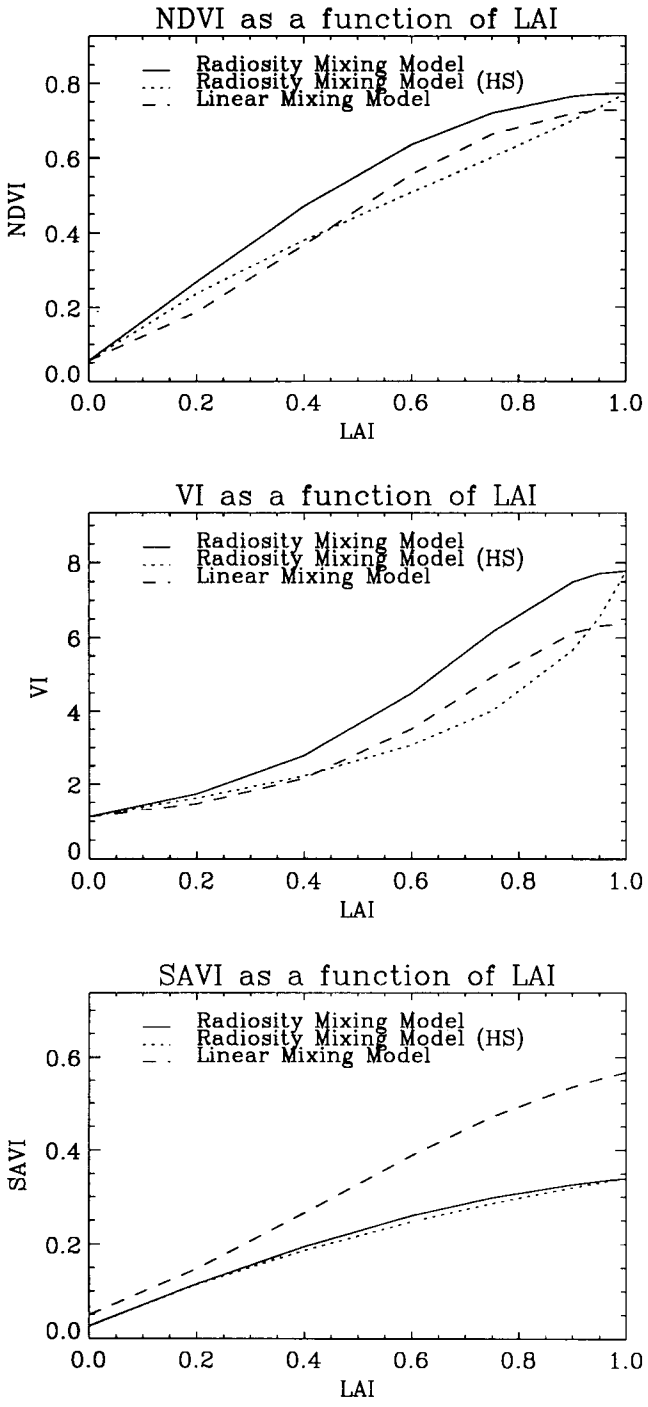

Figure 5. Three vegetation indices as a function of LAI for soil coefficients $a = 0.2$ and $b = 0.6$.

$$I_n^+ = C_1(1-b)^{n-1} + C_2(1+b)^{n-1}, \quad (19)$$

$$I_{N+1}^+ = \rho_s(C_3(1-b)^{N-1} + C_4(1+b)^{N-1}), \quad (20)$$

$$I_n^- = C_3(1-b)^{n-1} + C_4(1+b)^{n-1} - (1-\text{lai})^n E_0, \quad (21)$$

where C_1, C_2, C_3, C_4, and b are functions of ρ, τ, ρ_s, lai, and E_0. These expressions can be evaluated very quickly and spectral radiances can be obtained at different levels

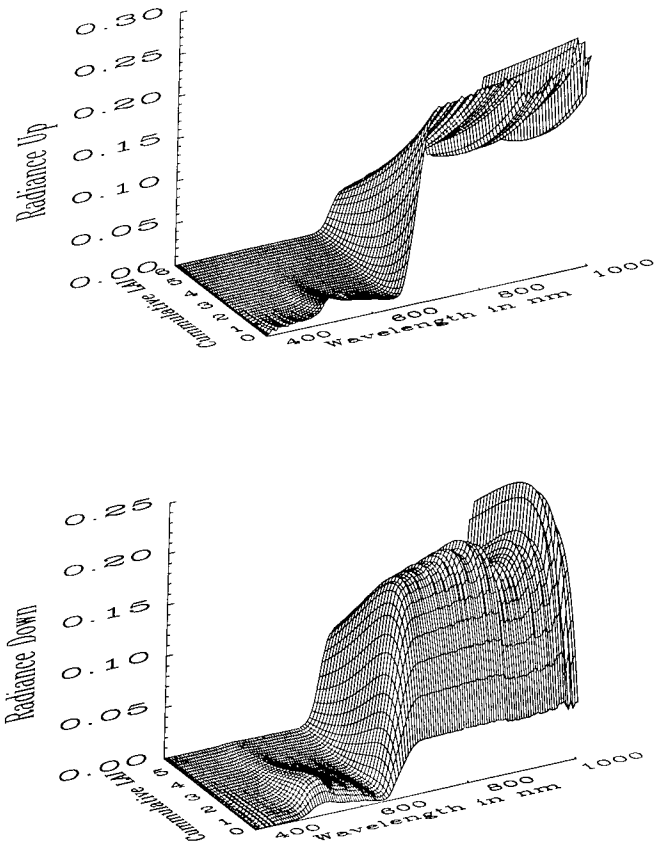

Figure 6. Spectral up and down radiances inside a 30-layer canopy with a leaf area index of 0.1 per layer and soil coefficients $a = 0.2$ and $b = 0.6$.

inside the canopy. Figure 6 shows an example of spectral radiances as a function of the downward cumulative leaf area index and wavelength in a 30-layer canopy with a leaf area index of 0.1 per layer and the cotton reflectance and transmittance characteristics. It takes only about 2 s to compute all radiances for a 30-layer canopy and 140 different wavelengths on a UNIX workstation (SUN SparcStation IPC) using the computer language IDL.

Vegetation Indices for a Layered Canopy

As for the single-layer model, we have shown that vegetation indices are nonlinear functions of the total leaf area index. In Figure 7 we show a plot of the RED and NIR reflectance of a 30-layer canopy as function of the total LAI. If we plot the data in a scatter diagram, it follows the trend observed experimentally by Huete et al. (1985). In Figure 8 we plot the three vegetation indices which have a steep rise for canopies with total LAIs between 0. and 2. and then saturate. This leads us to conclude that vegetation indices such as NDVI, VI, and SAVI are useful for canopy LAI studies up to about 2, but do not change enough to allow the retrieval of the LAI of denser canopies (LAI > 2). We expect that the use of radiosity based vegetation indices will

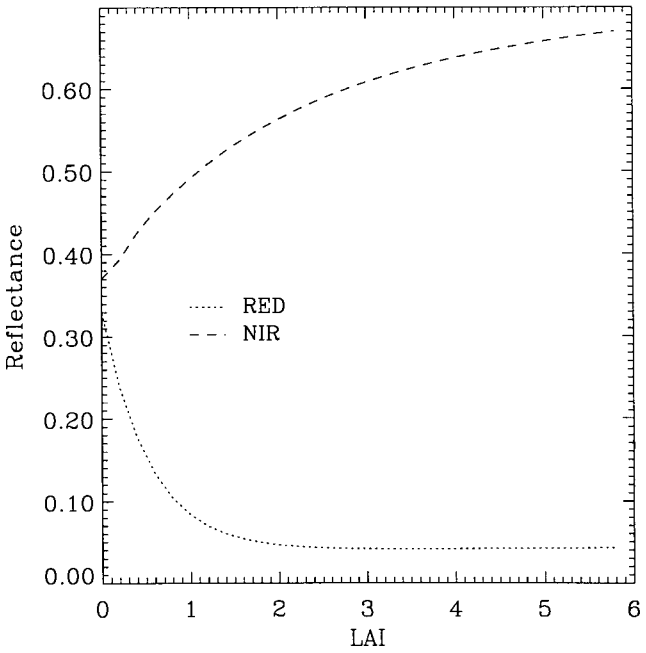

Figure 7. RED and NIR reflectance for a 30-layer canopy as a function of the toal leaf area index.

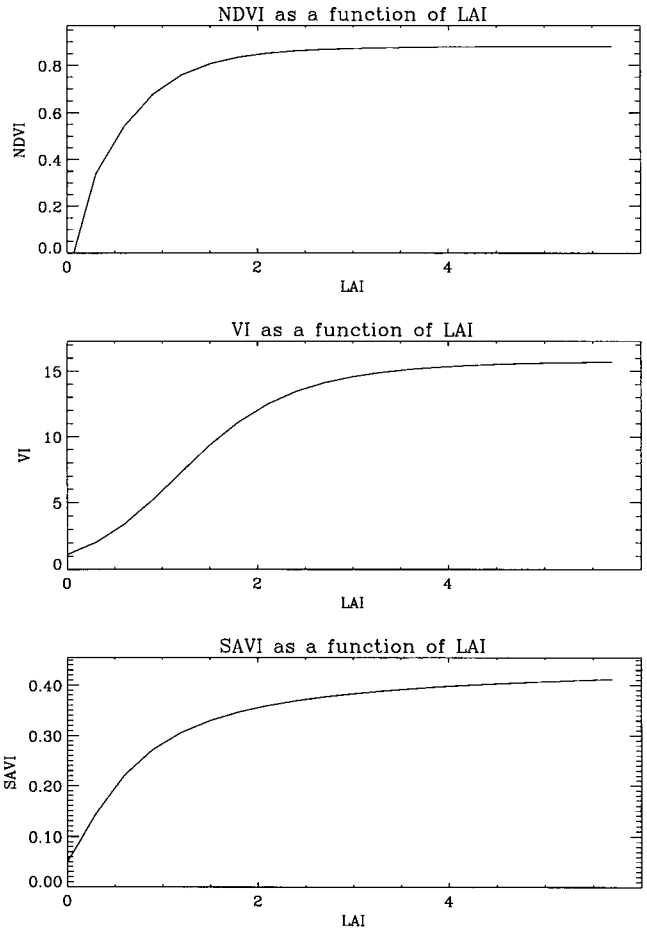

Figure 8. Three vegetation indices as a function of the total leaf area index of a 30-layer canopy for soil coefficients $a = 0.2$ and $b = 0.6$.

improve the retrieval of LAI since multiple scattering and transmission are included. It might, however, be necessary to develop vegetation indices for various leaf angle distributions and sun angles.

Spectral BRDF for a Layered Canopy

For a layered canopy with N layers the spectral BRDF is given by the equation in Borel et al. (1991)

$$f(\theta_i, \varphi_i; \theta_r, \varphi_r) = \frac{1}{E_0} \sum_{n=1}^{N+1} \frac{1}{\pi} [P_n^{\text{sunlit}}(\theta_r, \varphi_r) B_n^{\text{sunlit}} + P_n^{\text{shade}}(\theta_r, \varphi_r) B_n^{\text{shade}}], \quad (22)$$

where the radiosities B_n^{sunlit} for the sunlit top surface of the n-th layer are given by

$$B_n^{\text{sunlit}} = \begin{cases} \dfrac{B_n^+}{\text{lai}}, & \text{if } n = 1, \\ \rho E_0 + \dfrac{B_n^+}{\text{lai}} - \rho(1 - \text{lai})^{n-1} E_0, & \text{if } n = 2, 3, \ldots, N, \\ \rho_s E_0 + B_n^+ - \rho_s(1 - \text{lai})^{n-1} E_0, & \text{if } n = N+1, \end{cases} \quad (23)$$

and the radiosities B_n^{shadow} for the shaded top surfaces of the n-th layer are given by

$$B_n^{\text{shade}} = \begin{cases} 0, & \text{if } n = 1, \\ \dfrac{B_n^+}{\text{lai}} - \rho(1 - \text{lai})^{n-1} E_0, & \text{if } n = 2, 3, \ldots, N, \\ B_n^+ - \rho_s(1 - \text{lai})^{n-1} E_0, & \text{if } n = N+1, \end{cases} \quad (24)$$

where the radiosity B_n^+ is the layer-averaged radiosity of the upward pointing nth leaf layer and can be determined using Eq. (52) in Borel et al. (1991) as

$$B_n^+ = \begin{cases} \pi[I_n^+ - (1 - \text{lai}) I_{n+1}^+], & \text{if } n = 0, 1, \ldots, N, \\ \pi I_n^+, & \text{if } n = N+1. \end{cases} \quad (25)$$

Using raytracing, it is possible to compute the probabilities P_n^{sunlit} and P_n^{shade} for any illumination direction and view direction. For a 10-layer canopy with a layer lai of 0.1962, we computed the probabilities for an illumination direction of 30° and view angles from 0° to 65° in the principal plane. The probabilities are shown in Figure 9. Notice that, due to aliasing effects from the shadowing algorithm used by Borel (1988), the probability of seeing shadows is not equal to zero in the hot spot direction and also the probability of seeing a leaf is underestimated by about 25%. Therefore, e.g., we obtain $BP_1^{\text{sunlit}} \approx 0.15$ instead of 0.192. The spectral BRDF for this simple canopy is shown in Figure 10. The soil constants were $a = 0.2$ and $b = 0.6$. Notice the ridge produced by the hot spot effect for $\theta_r = 30°$. We

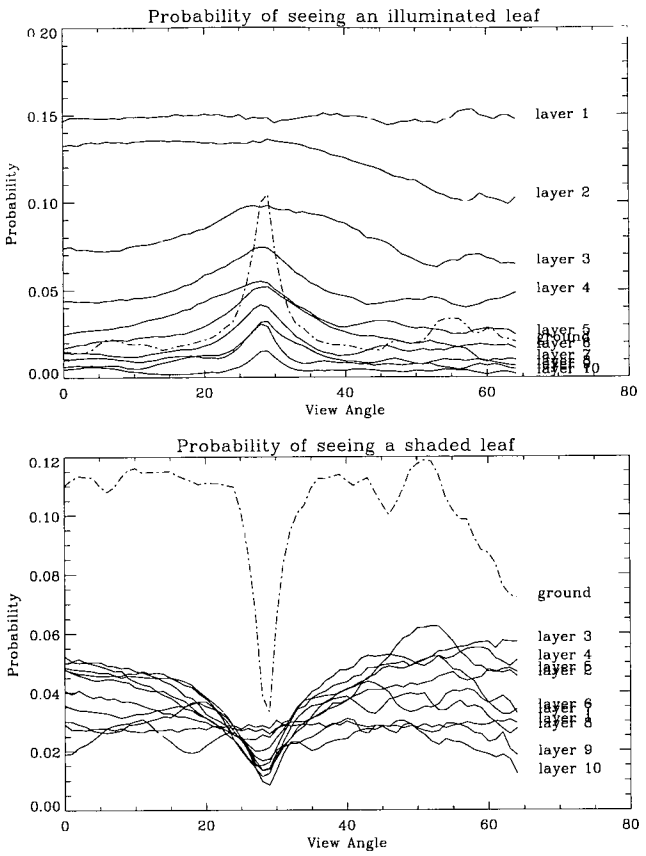

Figure 9. Probabilities of seeing sunlit and shaded leaves and ground as a function of view angle for an illumination direction of 30° in the principal plane.

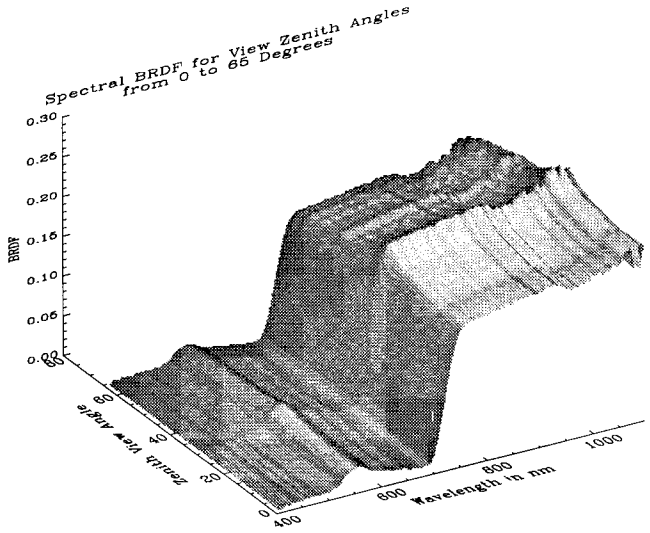

Figure 10. Spectral BRDF for a 10-layer canopy with a total LAI = 1.962.

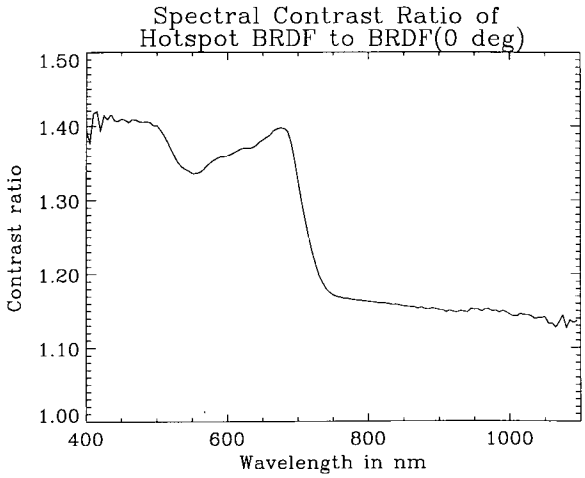

Figure 11. Contrast ratio as a function of wavelength for a 10-layer canopy with a total LAI = 1.962.

also found that the contrast ratio between the BRDF in the hot spot direction and zenith view angle

$$C = \frac{f(\theta_i, \varphi_i; \theta_i, \varphi_i)}{f(\theta_i, \varphi_i; \theta_r = 0^0, \varphi_r = 0^0)}, \tag{26}$$

is strongly dependent on the wavelength as shown in Figure 11. The contrast ratio seems to be proportional to $(1 - \rho)$, for example, for a low reflectance the contrast ratio is larger than for high reflectances. This is due to the fact that shadows are relatively darker when the reflectance and transmittance are low and are brightened up due to multiple reflections and transmission of light when ρ and τ are larger. We also computed the NDVI as a function of view angle and show the result in Figure 12. The NDVI does not change much with the viewing angle for this relatively dense canopy. This is due to the fact that the BRDF for a horizontal Lambertian leaf canopy reaches an asymptote for viewing angles away from the hot spot. For less dense canopies the NDVI depends more on the viewing angle as one can deduce from the NDVI curves for the hot spot direction and the non-HS direction of Figure 4.

NONLINEAR MIXING FOR ROUGH SURFACES

In the previous sections we have shown that nonlinear mixing is due to multiple reflections and transmission of light. Another important case of nonlinear mixing occurs when materials with different spectral reflectances compose a rough surface, for example, a plowed field with exposed rocks or well-mixed small particles of different minerals (see Singer and McCord, 1979). In this section we develop simple models to illustrate the magnitude of nonlinear effects.

Two-Facet Model

In Figure 13 a simple geometry for one period in a periodic rough surface is shown. The surface extends to infinity in the direction vertical to the cross section. Each surface has a fraction f of material 1 and a fraction

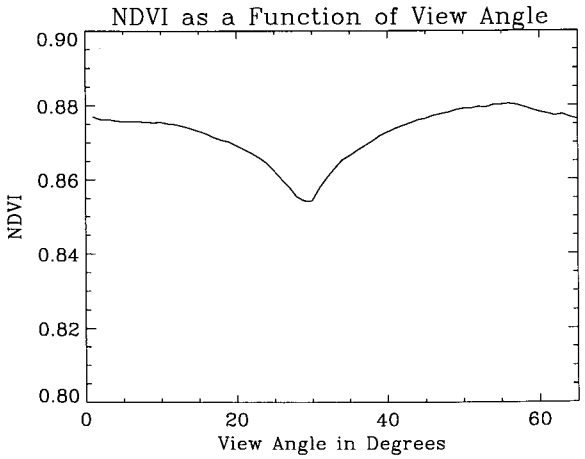

Figure 12. NDVI as a function of view angle.

$(1-f)$ of material 2. The average reflectance $\bar{\rho}$ per unit area is then given by

$$\bar{\rho} = f\rho_1 + (1-f)\rho_2, \tag{27}$$

where ρ_1 is the reflectance of material 1 and ρ_2 is the reflectance of material 2. The radiosity equations for vertical illumination can then be written as

$$B_1 = \bar{\rho}E_0 \cos\theta_1 + \bar{\rho}F_{12}B_2,$$
$$B_2 = \bar{\rho}E_0 \cos\theta_2 + \bar{\rho}F_{21}B_1, \tag{28}$$

where the view factors $F_{12} = F_{21} = F$. We assume that $\theta_1 + \theta_2 = \bar{u}$, and therefore all expressions can be written with $\theta_1 = \theta$ alone. The view factor F between the surfaces can be determined by using the crossed string method (see Hottel and Sarofim, 1967), which is illustrated in Figure 14. The view factor between two infinite strips with areas S_1 and S_2:

$$S_1F_{12} = \frac{\overline{AD} + \overline{BC} - \overline{AC} - \overline{BD}}{2}, \tag{29}$$

Figure 13. Geometry of a rough surface composed of two materials.

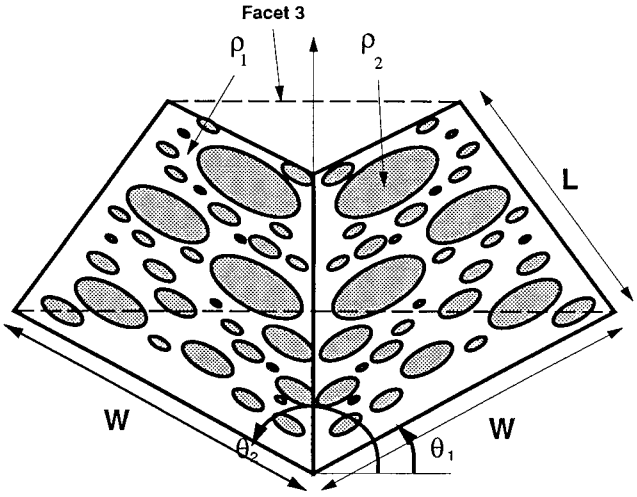

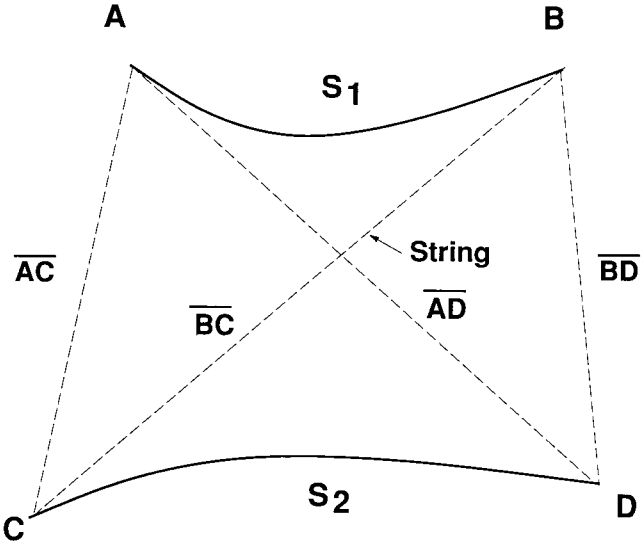

Figure 14. Crossed string method to compute view factors.

where $\overline{AD}$ is the length between the points A and D, etc. Thus we have

$$F = (1 - \cos\theta), \tag{30}$$

where θ is the surface slope measured from the horizontal plane and the geometry is shown in Figure 13. The solution of Eq. (28) is then given by

$$B = B_1 = B_2 = \frac{\bar{\rho}\cos\theta\, E_0 + \bar{\rho}^2 F \cos\theta\, E_0}{1 - \bar{\rho}^2F^2}. \tag{31}$$

Next we need to determine the radiosity leaving the two facets. We can define an imaginary surface 3 covering the facets 1 and 2. Using the crossed string method the view factors between facets 1 and 2 to facet 3 are given by

$$F_{31} = F_{32} = \frac{W + 2W\cos\theta - W}{2W} = \cos\theta, \tag{32}$$

and the radiosity over the two facets is then

$$B_3 = B_1F_{31} + B_2F_{32} = 2BW\cos\theta. \tag{33}$$

By definition the reflectance of any surface is given by the ratio of the outgoing irradiance (or radiosity) over the incident irradiance. For the periodic surface this ratio can be computed using the radiances going through the imaginary facet 3. The outgoing irradiance is equal to the radiosity B_3 and the incident irradiance depends on the width of facet 3 and is equal to $E_0 2\cos\theta$. For normal illumination and arbitrary viewing direction the reflectance is

$$\rho_{\text{radiosity}}(\theta_i = 0, \varphi_i = 0; \theta_r, \varphi_r) = \frac{B_3}{2\cos\theta\, E_0} = \frac{B}{E_0}$$
$$= \frac{\bar{\rho}\cos\theta + \bar{\rho}^2(1-\cos\theta)\cos\theta}{1 - [\bar{\rho}(1-\cos\theta)]^2}, \tag{34}$$

where $\rho_{\text{radiosity}}$ is the radiosity derived reflectance. For a linear mixing model the reflectance of a two component model is given by

$$\rho_{\text{linear}} = \frac{\overline{\rho}\cos\theta\, E_0}{E_0} = \overline{\rho}\cos\theta. \tag{35}$$

Experimental Validation of the Two-Facet Model

To validate the two-facet model, we built a mechanical model. An optical bench was used to hold two aluminum plates covered with colored paper and backed by black paper to eliminate possible multiple reflections between aluminum and paper. A fiberoptic spectrometer head was mounted on a copy stand and its field-of-view was carefully centered. The two facets were positioned towards the sun such that both faces were illuminated equally and specular reflections from the paper were kept as small as possible. The spectrometer was calibrated using a white calibration target which was put onto the edges of the two facets to measure E_0. The useful range of the spectrometer ranged from 400 nm to 900 nm with a spectral sample spacing of 1.4 nm to 1.5 nm. The angle θ can be changed by sliding two holders on an optical bench into predetermined positions. The selected angles were $\theta = 75°$, 65°, 60°, 50°, and 36°. Several colored papers and combinations of two different colored papers facing each other were measured. For each paper we measured the single surface reflectance ρ_{single} with the same spectrometer and an integrating sphere. To illustrate the nonlinear effect, we plot the multiple surface reflectance ρ_{multi} as a function of the slope corrected single surface reflectance $\rho_{\text{single}}\cos\theta$ (see Fig. 15). In each plot we show three curves: measurement, radiosity computed [see Eq. (34)], and linear mixing [see Eq. (35)] for brown paper. No scaling or shifting was performed on the measured reflectances. This representation allows us to readily estimate the quantity by which the reflectance changes due to multiple reflections, for example, for $\theta = 75°$ the multiple scattering component adds 0.5 to a single scattering contribution of 0.24 in the case of a single scattering reflectance of 0.9. Even for an angle of 50° the multiple scattering component is still greater than 0.25. The measurement and radiosity computed curves agree very well, except for $\theta = 36°$. Equation (34) can be solved for the slope angle θ:

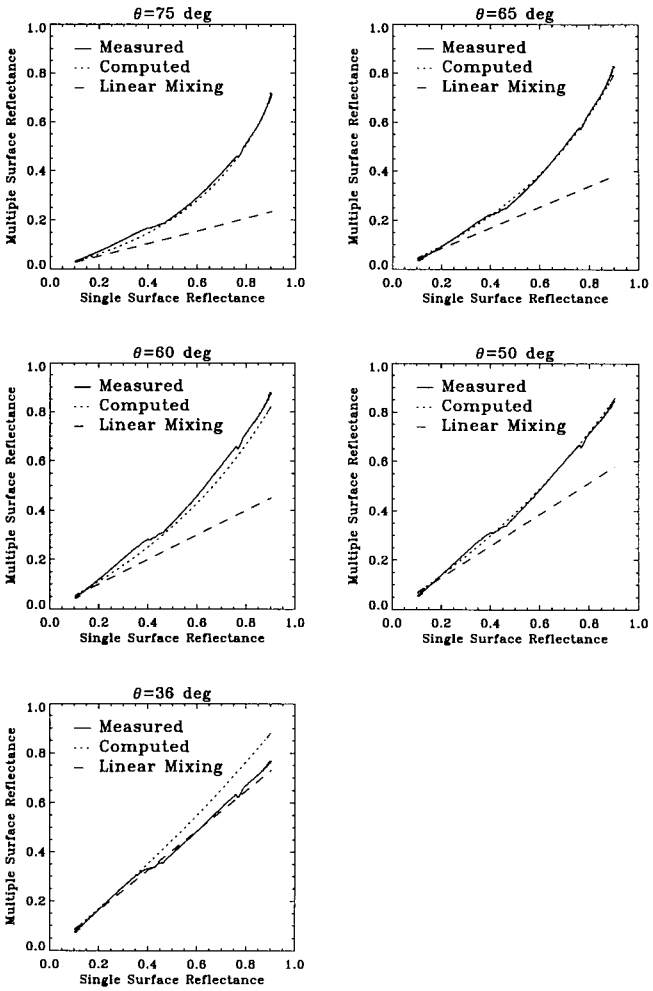

Figure 15. Multiple surface reflectance versus single surface reflectance of a two-facet structure. Each plot shows measured, radiosity computed, and linear mixing model curves for facet angles: $\theta = 75°$, 65°, 60°, 50°, and 36° and brown paper.

$$\theta(\rho_{\text{single}},\rho_{\text{multi}}) = \cos^{-1}\left[1 - \frac{\rho_{\text{single}} - 1 + \sqrt{(1+\rho_{\text{single}})^2 + 4\rho_{\text{multi}}(\rho_{\text{multi}} - \rho_{\text{single}} - 1)}}{2\rho_{\text{single}}(1-\rho_{\text{multi}})}\right]. \tag{36}$$

Using Eq. (36) and the measured single surface reflectances ρ_{single} and multi surface reflectances ρ_{multi} from 400 nm to 900 nm, we compute the slope angle θ. The averages for the estimated angles $\langle\theta\rangle$ over the spectrum for the listed angles θ are: 73.67°, 65.64°, 55.46°, 52.67°, and 50.56°. The average estimated angles are within 5° of the actual slope angles for the first four measurements and off by 16° for the fifth measurement. The differences could be due to mechanical problems, calibration problems, scattering from other surfaces, BRDF effects of the paper, etc. The conclusion of the experiment is, however, that indeed multiple scattering between bright surfaces will lead to nonlinear mixing and that the radiosity method can be used to quantify the nonlinear effect.

The implications for geological remote sensing are that natural bright and very rough surfaces can have a very different spectrum than laboratory measured

polished or smooth samples. It remains to be investigated how linear unmixing algorithms are affected by the nonlinear mixing.

Numerical Example of a Two-Component Surface

We calculated the reflectances $\rho_{\text{radiosity}}$ and $\bar{p}$ for two laboratory spectra (Goetz, 1992) for alunite and halloysite measured from 0.3 μm to 2.6 μm in steps of 5 nm. We let the fraction f vary from 0% to 100% in steps of 33.33% and set the slope angle to 40°. The resulting spectra are shown in Figure 16. Notice the difference between the linear and the radiosity based nonlinear mixing model. Note that even when only one material is present $f=0.$ and $f=1.$, there is a difference in the spectra because of multiple reflections between the facets. We assume that the reflectance spectra used were measured for a flat sample.

Numerical Example of a Three-Component Surface

It has been noted by several researchers (e.g., Nash and Conel, 1974; Hapke, 1981; Johnson et al., 1983) that nonlinear mixing occurs when spectra of well mixed or aggregates of minerals are measured. We can use the above model to study the behavior of the reflectance at particular wavelenths for a three-component (ternary) surface. The average reflectance $\bar{p}$ per unit area is then given by

$$\bar{p} = f_1\rho_1 + f_2\rho_2 + (1-f_1-f_2)\rho_3, \tag{37}$$

where the fractions f_1, f_2, and $(1-f_1-f_2)$ add up to unity. To demonstrate nonlinear mixing, we selected laboratory spectra of alunite, halloysite, and kaolinite. The reflectance spectra as obtained from Goetz (1992) are shown in Figure 17. To show that nonlinear mixing occurs, we selected an absorption feature of alunite and also kaolinite at 1.435 μm and one for halloysite at 1.91 μm. The slope was selected to be 70° to simulate through mixing, for example, mixed powders as shown in Nash and Conel (1974). Figure 18 shows the reflectance in a triangle with the abundances of kaolinite and halloysite as x and y axes. Very similar nonlinear effects as in Nash and Conel (1974) are observed here. Extending the two- and three-component reflectance model to an N component model can be done as follows:

$$\bar{p} = \sum_{i=1}^{N} f_i\rho_i, \quad \text{where} \sum_{i=1}^{N} f_i = 1. \tag{38}$$

The reflectance of an N-component faceted surface is then obtained from Eq. (34). We speculate that nonlinear effects have to be taken into account when spectral unmixing is done for wavelengths in absorption features. The nonlinear unmixing should be possible since only one additional parameter, the view factor F has to be determined. As we have noted earlier, the view factor is related to the angle between the surface normal and nadir of the surface and thus could be used as a single parameter characterizing the surface roughness.

Figure 16. Spectra of mixtures of alunite and halloysite in a sloped surface model $\theta=40°$ as fractions of halloysite (0%, 33.3%, 66.6%, and 100%).

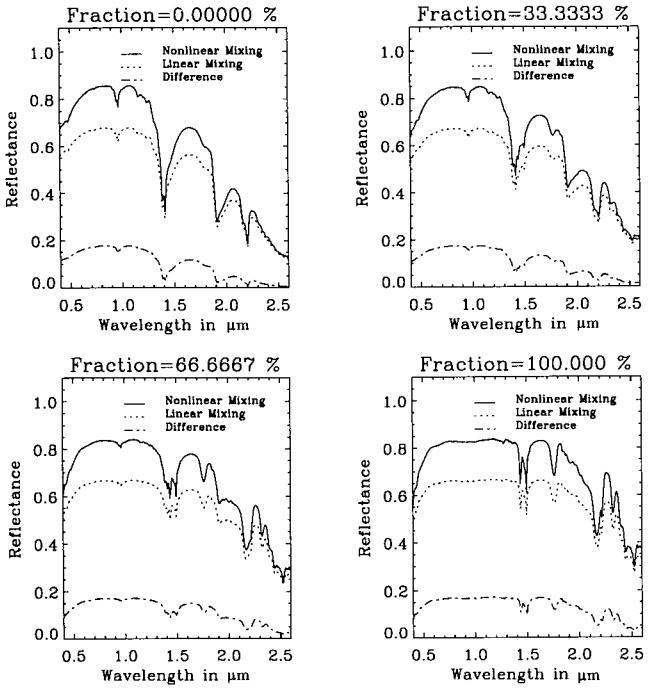

Figure 17. Reflectance spectra of alunite, halloysite, and kaolinite minerals.

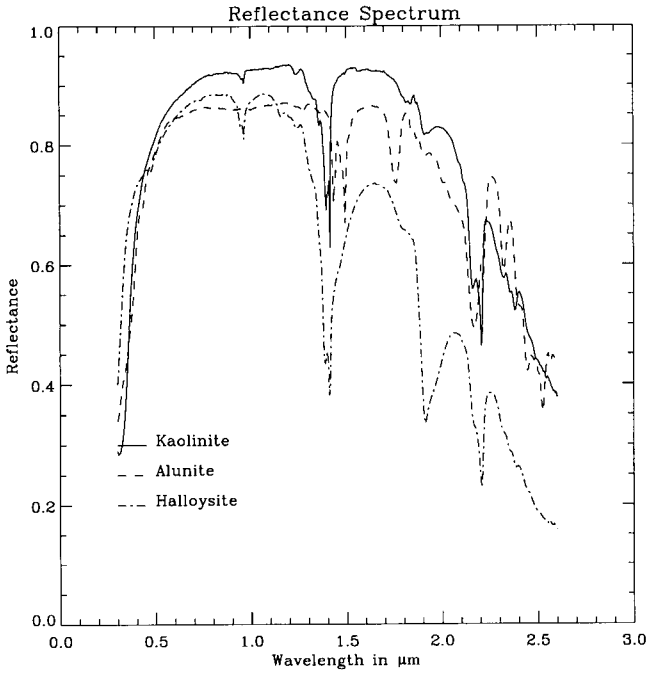

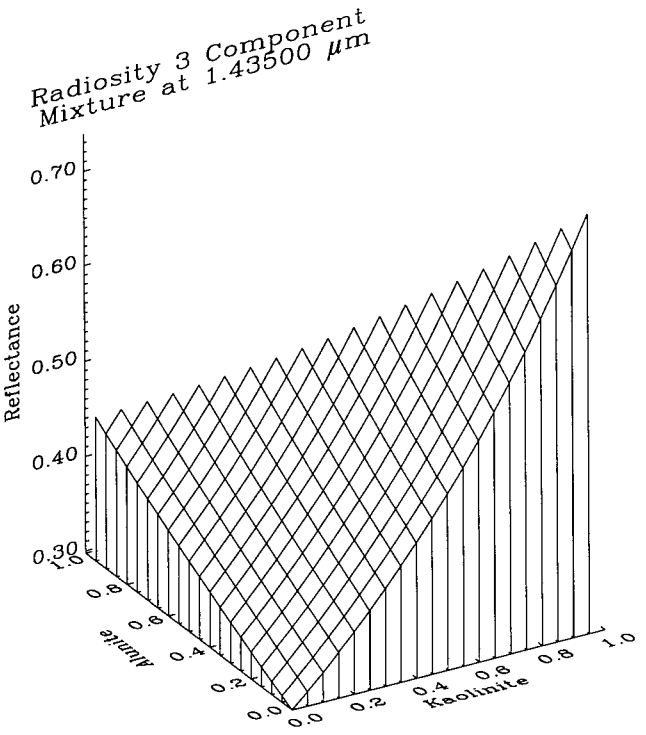

(a)

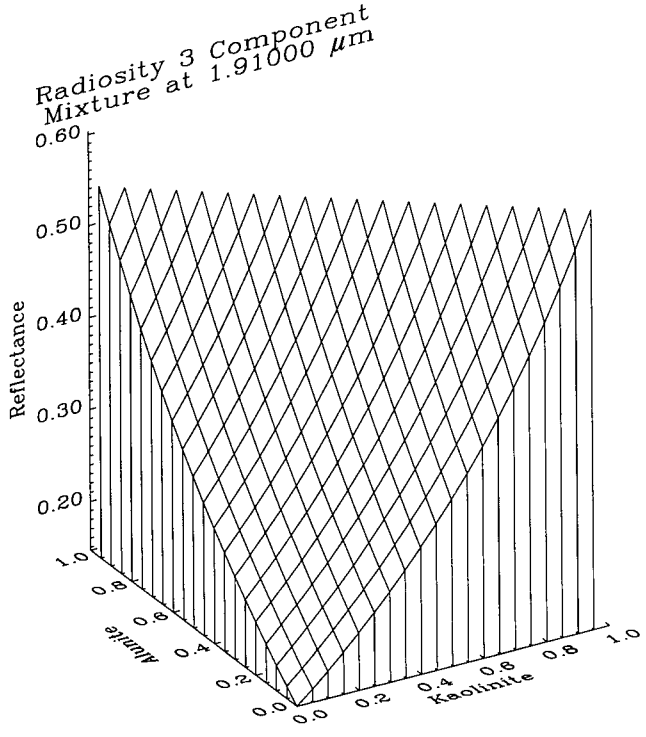

(b)

Figure 18. Reflectance for a ternary mixture of alunite, halloysite, and kaolinite at selected wavelengths for $\theta = 70°$.

CONCLUSIONS

We have developed several simple models to demonstrate that nonlinear mixing occurs when multiple scattering effects are considered. First, a one-layer model of vegetation above ground was shown to exhibit dramatically increased reflectance in the near-infrared due to multiple reflections between the leaves and soil. The reflectance can double in our model calculations. Then we considered the effect of the nonlinear mixing on several vegetation indices and found a nonlinear relationship between vegetation indices and the leaf area index. We then turned to a layered canopy and showed that the up- and downward radiances inside a canopy have different spectral content. We found that vegetation indices for dense canopies vary nonlinearly with total LAI. Using a raytracing method to estimate probabilities for seeing illuminated and shaded leaves or ground, we calculated the spectral BRDF for a slice in the principal plane. We also showed that the contrast ratio between the BRDF in the hot spot direction over the BRDF in the nadir direction is greatest for low reflectances and decreases for higher reflectances, for example, in the green and near infrared. For a dense canopy we found that the NDVI depends weakly on the view angle.

A simple model for a rough surface composed of different minerals arranged on two tilted facets was developed. An experiment using two inclined paper facets illuminated by sunlight and a spectrometer measuring the reflectance in the visible and near infrared showed very good agreement between model and measurement. The reflectance of a two-facet surface as a function of binary and ternary mixtures showed that multiple reflections change the shape of the spectrum where large reflectances occur and that intimate mixtures produce nonlinear mixing surfaces near absorption features.

Radiosity based models should be investigated in more detail theoretically and experimentally. Further investigations may lead to improved vegetation indices and possibly to nonlinear unmixing algorithms. The radiosity method is capable of modeling very complicated structures as shown in Borel et al. (1991) and Goel et al. (1991). Effects from scattered skylight should also be taken into account as well as atmospheric effects (see Huete and Jackson, 1988). We believe that the extended radiosity method (Borel and Gerstl, 1991) could be used to model volumetric nonlinear mixing of plankton or sediments in water and possibly be applied to generate a biochemical leaf reflectance scattering model. Further applications could lie in the modeling of multiple scattering between layered clouds and the ground surface. A possible application for Earth radiation budget sensors lies in better quantifiable fractional cloud covers.

A very important application for the near future lies in improving the vegetation indices for current sensors such as AVHRR and Landsat TM. We expect many new applications in the era of EOS for the planned high-resolution imaging spectrometers such as MODIS (Salomonson et al, 1989) and high-resolution spectrometers (Goetz, 1987; Dozier and Goetz, 1989).

This research was supported by NASA's Remote Sensing Science (RSS) Program under a project to investigate the applications for the radiosity method to remote sensing. We are grateful to Ghassem Asrar, Diane Wickland, and Jon Ranson from NASA for their support. We thank Susan Ustin from the University of California at Davis for lending us her spectrometer and integrating sphere to perform the validation experiments. Karl Staenz from the Canadian Centre for Remote Sensing measured the cotton leaf reflectance and transmittance during the MAC-BRDF experiment in Maricopa, Arizona. Finally we are extremely grateful to two summer students: Dirk-Udo Eisser and Jochen Glas from the Polytechnical University of Konstanz, Germany. Both designed and built the setup for the two-facet experiment and measured the reported reflectances. We also acknowledge earlier contributions of Bill Powers, Los Alamos National Laboratory, to the analytical solution of the N-layer model.

REFERENCES

Asrar, G. (1989), *Theory and Applications of Optical Remote Sensing*, Wiley, New York, Chichester, Brisbane, Toronto, Singapore.

Baret, F., and Guyot, G. (1991), Potentials and limits of vegetation indices for LAI and APAR assessment, *Remote Sens. Environ.* 35:161–173.

Borel, C. C. (1988), Models for backscattering of millimeter waves from vegetative canopies, Ph.D. thesis, University of Massachusetts, September.

Borel, C. C., and Gerstl, S. A. W. (1991), Simulation of partially obscured scenes using the radiosity method, *Proc. SPIE* 1486:271–277.

Borel, C. C., Gerstl, S. A. W., and Powers, B. J. (1991), The radiosity method is optical remote sensing of structured 3-d surfaces, *Remote Sens. Environ.* 36:13–44.

Cihlar, J., St.-Saurent, L., and Dyer, J. A. (1991), Relation between the normalized difference vegetation index and ecological variables, *Remote Sens. Environ.* 35:279–298.

Dozier, J., and Goetz, A. F. H. (1989), HIRIS–EOS instrument with high spectral and spatial resolution, *Photogrammetrica* 43(3 / 4):167–180.

Gerstl, S. A. W., and Borel, C. C. (1990), Principles of the radiosity method for canopy reflectance modeling, in *Proc. Int. Geoscience and Remote Sensing Symposium*, 20–24 May, Vol. 3, pp. 1735–1737.

Goel, N. S. (1988), Models of vegetation canopy reflectance and their use in estimation of biophysical parameters from reflectance data, *Remote Sens. Rev.* 4(1):221.

Goel, N.S., Rozehnal, I., and Thompson, R. L. (1991), A computer graphics based model for scattering from objects of arbitrary shapes in the optical region, *Remote Sens. Environ.* 36:73–104.

Goetz, A. F. H. (1987), High-resolution imaging spectrometer (HIRIS)—instrument panel report, NASA, Earth Observation System Volume IIc, 1987.

Goetz, A. F. H. (1992), *SIPS User's Guide: Version 1.2*, Report Center for the Study of Earth from Space (CSES), Univ. of Colorado, September, p. 89.

Green, O. R. (1991), *Proceedings of the Third Airborne Visible / Infrared Imagine Spectrometer (AVIRIS) Workshop*, 20–24 May, JPL Publication 91-28.

Hapke, B. (1981), Bidirectional reflectance spectroscopy: 1. Theory, *J. Geophys. Res.* 86(B4):3039–3054.

Hottel, H. C., and Sarofim, A. F. (1967), *Radiative Transfer*, McGraw-Hill, New York.

Huete, A. R. (1986), Separation of soil–plant mixtures by factor analysis, *Remote Sens. Environ.* 19:237–251.

Huete, A. R., and Jackson, R. D. (1988), Soil and atmosphere influences on the spectra of partial canopies, *Remote Sens. Environ.* 25:89–105.

Huete, A. R., Jackson, R. D., and Post, D. F. (1985), Spectral response of a plant canopy with different soil backgrounds, *Remote Sens. Environ.* 17:37–53.

Jackson, R. D. (1983), Spectral indices in *N*-space, *Remote Sens. Environ.* 13:409–421.

Jasinski, M. F. (1990), Sensitivity of the normalized difference vegetation index to subpixel canopy cover, soil albedo, and pixel scale, *Remote Sens. Environ.* 32:169–187.

Johnson, P. E., Smith, M. O., Taylor-George, S., and Adams, J. B. (1983), A semiempirical method for analysis of the reflectance spectra of binary mineral mixtures, *J. Geophys. Res.* 88:3557–3561.

Kauth, R. J., and Thomas, G. S. (1976), The Tasseled Cap—a graphic description of the spectral-temporal development of agricultural crops as seen by Landsat, in *Proc. Symp. on Machine Proc. of Remotely Sensed Data*, Purdue Univ., West Lafayette, IN, pp. 41–51.

Nash, D. B., and Conel, J. E. (1974), Spectral systematics for mixtures of powdered Hypersthene, Labradorite and Ilmenite, *J. Geophys. Res.* 79(11):1615–1621.

Roberts, D. A. (1991), Separating spectral mixtures of vegetation and soils, Ph.D. thesis, University of Washington, June.

Roberts, D. A. (1992), private communication.

Roberts, D. A., Adams, J. B., and Smith, M. O. (1990), Predicted distribution of visible and near-infrared radiant flux above and below a transmittant leaf, *Remote Sens. Environ.* 34:1–17.

Roberts, D. A., Smith, M. O., Adams, J. B., and Gillespie, A. R. (1991), Leaf spectral types, residuals, and canopy shade in an AVIRIS image, in *Proc. 3rd Airborne Visible / Infrared Imaging Spectrometer (AVIRIS) Workshop*, 20–21 May, JPL Publication 91-28, Pasadena, CA.

Rushmeier, H. E., and Torrance, K. E. (1987), The zonal method for calculating light intensities in the presence of a participating medium, *SIGGRAPH Proc.*, 21(4):293.

Salomonson, V. V., Barnes, W. L., Maymon, P. W., Montgomery, H. E., and Ostrow, H. (1989), MODIS: advanced facility for studies of the Earth as a system, *Trans. Geosci. Remote Sens.* 27(3):145–153.

Satterwhite, M. B., and Henley, J. P. (1987), Spectral characteristics of selected soils and vegetation in northern Nevada and their discrimination using band ratio techniques, *Remote Sens. Environ.* 23:155–175.

Singer, R. B., and McCord, T. B. (1979), Mars: large scale mixing of bright and dark surface materials and implications for analysis of spectral reflectance, *Proc. Planet. Sci. Conf., 10th*, 2:1835–1848.

Smith, M. O., Ustin, S. L., Adams, J. B., and Gillespie, A. R. (1990a), Vegetation in deserts: I. A regional measure of abundance from multispectral images, *Remote Sens. Environ.* 31:1–26.

Smith, M. O., Ustin, S. L., Adams, J. B., and Gillespie, A. R. (1990b), Vegetation in deserts: II. Environmental influences on regional abundance. *Remote Sens. Environ.* 31: 27–52.

Staenz, K. (1991), Licor measured conical / bi-hemispherical spectral reflectance and transmittance spectra of cotton, private communication.

Tucker, C. J. (1979), Red and photographic infrared linear combinations to monitor vegetation, *Remote Sens. Environ.* 8:127–150.

Vane, G., and Goetz, A. F. H. (1988), Terrestrial imaging spectroscopy, *Remote Sens. Environ.* 24:1–29.

Williams, D. L. (1991), A comparison of spectral reflectance properties at the needle, branch and canopy level for selected conifer species, *Remote Sens. Environ.* 35:79–93.